Landslides (2009) 6:181–190
DOI 10.1007/s10346-009-0157-4
Received: 14 October 2008
Accepted: 8 May 2009
Published online: 3 June 2009

William H. Schulz · Jonathan P. McKenna · John D. Kibler · Giulia Biavati

Relations between hydrology and velocity of a continuously moving landslide—evidence of pore-pressure feedback regulating landslide motion?

Abstract We measured displacement, pore-water pressure, and climatic conditions for 3 years at the continuously moving Slumgullion landslide in Colorado, USA. The landslide accelerated when pore-water pressure increased within the landslide body, but this occurred as pore-water pressure decreased along the landslide margin. The decrease probably occurred in response to shear-induced soil dilation at rates greater than pore-pressure diffusion and likely increased resistance to shear displacement and resulted in landslide deceleration. This dilative strengthening has been experimentally observed and explained theoretically, but not previously identified during field studies. Although landslide displacement should have exceeded that required to achieve critical-state density of shear boundaries, observed relocation of these boundaries indicates that shearing is episodic at fixed locations, so it permits renewed dilative strengthening when "fresh" soil is sheared. Thus, dilatant strengthening may be a considerable mechanism controlling landslide velocity, even for landslides that have continuously moved great distances.

Keywords Landslide · Slumgullion · Dilation · Pore-water pressure · Velocity · Colorado · USA

Introduction

Landslides move at rates that range from centimeters per year to meters per second, and movement may be continuous for many years, may be interrupted by periods of dormancy, or may be short-lived followed by permanent landslide inactivity. The different movement characteristics present different hazards. For example, landslides that move very slowly and episodically create little safety hazard and may be occupied by homes and related infrastructure that suffer periodic damage, whereas landslides that move rapidly commonly destroy structures and cause human fatalities. To permit accurate identification of landslide hazards, the factors controlling landslide movement characteristics must be understood. Factors that may affect landslide velocity include internal and boundary pore-water pressures, landslide inertia, and material properties such as strength, viscosity, and relative density.

Steady pore-water pressures have been observed to result in steady landslide movement (e.g., Baum and Reid 2000; Coe et al. 2003). Unsteady movement has been attributed to changing pore-water pressures such as produced by changing precipitation and snowmelt conditions (e.g., Prior and Stephens 1972; Hutchinson et al. 1974; Iverson and Major 1987; Baum et al. 1993; Fleming et al. 1999; Corominas et al. 2005), undrained loading of landslide material (Hutchinson et al. 1974; Grainger and Kalaugher 1987), and erosion of material that resisted landslide movement (Grainger and Kalaugher 1987). Viscous resistance to shear deformation may also affect landslide velocity (e.g., Locat and Demers 1988; Vulliet and Hutter 1988; Tika et al. 1996; Lemos 2004; Corominas et al. 2005; van Asch et al. 2007).

Landslide velocity may also be governed by material properties that change due to landslide displacement. In most cases, these changing properties directly affect pore-water pressures, which then directly affect landslide displacement characteristics. For example, continuous, long-term landslide motion may be partly due to pore-water pressure changes from dilation and consolidation of fine-grained landslide material as it overrides asperities along the basal rupture surface (Keefer and Johnson 1983; Baum and Johnson 1993; van Asch et al. 2007). Many styles of landslide movement may be explained following Reynolds' (1885) and Casagrande's (1936) approaches, which invoke shear-induced dilation and contraction of granular material (soil) that cause changes in pore-water pressure resulting in modification of landslide velocity. For example, it has been proposed that rapid, long-distance landslide movement results from contraction of loose soil during shear displacement and consequent pore-water pressure rise and effective liquefaction of sheared landslide material (e.g., Sassa 1984; Iverson et al. 2000; Wang and Sassa 2003). It has also been proposed that this type of movement results from dilation and mixing of dense soil during shear in the presence of ample groundwater and/or surface water or after total displacement is sufficient to reach steady-state porosity (e.g., Casagrande 1936; Johnson and Rodine 1984; Fleming et al. 1989; Gabet and Mudd 2006). Decelerating, short-distance landslide movement has been ascribed to dilation of dense soil during shear and consequent pore-water pressure drop that increases effective stress and shear resistance along the landslide base (e.g., Iverson et al. 1997, 2000; Moore and Iverson 2002; Iverson 2005). Similarly, semicontinuous landslide motion over long periods (months–years) may be due to dilation during shear displacement that causes pore-water pressure to drop, effective stress to rise, and the landslide to stop. Subsequent consolidation allows shear-induced dilation to recur when pore-pressures rise sufficiently to trigger renewed movement. This behavior has been observed during laboratory (Moore and Iverson 2002), field-scale (e.g., Iverson et al. 2000), and theoretical studies (Schaeffer and Iverson 2009). However, as noted by Moore and Iverson (2002) and Iverson (2005), sufficient landslide displacement will cause dilation to steady-state porosity and deceleration associated with dilation will no longer occur; runaway landslide acceleration may follow.

Because of the differences in the current understanding of landslide motion, landslide case studies provide particularly useful information. However, long-term studies of continuously moving landslides are rare. The Slumgullion landslide, located in southwestern Colorado, USA (Fig. 1), is one exception. The landslide has been studied in detail and appears to have been continuously active for about the last 300 years (Crandell and Varnes 1961; Varnes and Savage 1996) with total displacement on the order of hundreds of meters (Coe et al. 2008). We performed field and laboratory tests of material properties and monitoring of its

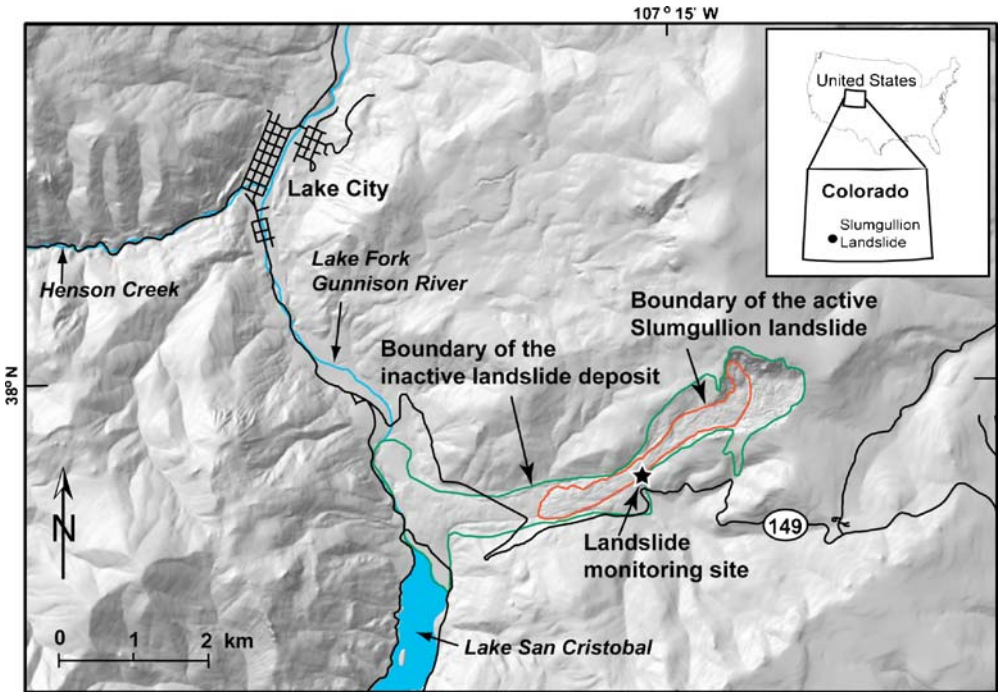

Fig. 1 Shaded relief map showing the locations of the Slumgullion landslide and monitoring site. Boundaries of the inactive and active landslides are from Madole (1996) and Fleming et al. (1999), respectively. Topography of the active landslide is from Messerich and Coe (2003)

displacement, pore-water pressures, and climate during a 39-month period. Our work was directed at identifying mechanisms responsible for continuous, nearly steady landslide motion as has been observed at this landslide previously (Savage and Fleming 1996; Fleming et al. 1999; Coe et al. 2003) with emphasis on climatic effects and interaction of pore-water pressure and landslide displacement.

Setting

The Slumgullion landslide is a translational debris slide (classification of Cruden and Varnes 1996) and consists of an active part contained within a larger inactive landslide deposit (Figs. 1 and 2). The landslide was for many years called an earthflow (e.g., Crandell and Varnes 1961; Varnes and Savage 1996). However, the term flow was used improperly because nearly all displacement occurs by translational sliding along bounding shear surfaces (Fleming et al. 1999), so the term slide (Cruden and Varnes 1996) is appropriate, and the term debris is appropriate, rather than earth, because the landslide appears to consist of >20% coarse-grained particles (Schulz et al. 2007b). We refer to Slumgullion as a landslide herein. Radiocarbon dating of trees buried beneath the toe of the inactive landslide suggests that it was active about 800–900 years ago (Madole 1996). The landslide deposit is derived from Tertiary basalt, rhyolite, and andesite, much of which has been highly altered by hydrothermal activity (Lipman 1976; Sharp et al. 1983; Diehl and Schuster 1996; Fleming et al. 1999). The active landslide is 3.9 km long and has an estimated volume of 20×10^6 m^3 (Parise and Guzzi 1992), average thickness of about 13 m (Parise and Guzzi 1992), and average slope of 8°.

Landslide displacement occurs mainly along bounding shear surfaces or within shear zones a few meters wide. Shear zones are expressed at the ground surface as en echelon fractures. Excavation of fractures and discrete shear surfaces revealed that they consist of tabular clay layers up to a few centimeters wide with slickensided surfaces. These tabular clay layers have been referred to as dikes at this landslide and others and were thought to be intruded through the landslide debris (Fleming and Johnson 1989; Fleming et al. 1999). The shear surfaces and zones are commonly located between the outside edges and peaks of flank ridges. Both dormant and active flank ridges occur along the landslide margins (Fleming et al. 1999; Schulz et al. 2007a). The active flank ridges are generally 2–8 m high with steeply sloping sides (40–60°), may have a sharp peak or flat top, and appeared to consist of much looser, finer-grained soil than neighboring soil within the landslide. These ridges likely result from soil dilation within a shear zone, similar to marginal shear zones at other landslides (Fleming and Johnson 1989; Baum et al. 1993) and along strike-slip tectonic faults (Rudnicki 1984; Johnson and Fleming 1989; Johnson 1995; Fleming et al. 1997).

Fleming et al. (1999) performed detailed mapping of the landslide and concluded that its annual displacement had been about constant during the preceding 100 years and that the landslide consists of several independent kinematic units that can have differing velocities. These units are generally separated by discrete shear surfaces or narrow zones across which most differential displacement occurs. Fleming et al. (1999) measured average annual velocities of 0.2–7.4 m/year (0.05–2.0 cm/day) with lowest velocity at the landslide head (<1 m/year, 0.3 cm/day), low velocity at the toe (<2 m/year, 0.5 cm/day), and greatest velocity (>7 m/year, 1.9 cm/day) where the landslide is narrowest and steepest. They found that velocity varies seasonally, presumably due to changes in pore-water pressures. Savage and Fleming (1996) measured continuous landslide displacement with seasonally varying rate during part of 1993. Coe et al. (2003) performed periodic surveying of surface monuments distributed across the landslide and hourly monitoring at two locations of landslide displacement, air and soil temperature, snow depth, rainfall, soil–water content, and groundwater pressures within an apparently perched aquifer. They found that the landslide moved fastest during spring and summer and slowest during winter. They identified generally direct, positive correlation between pore-water

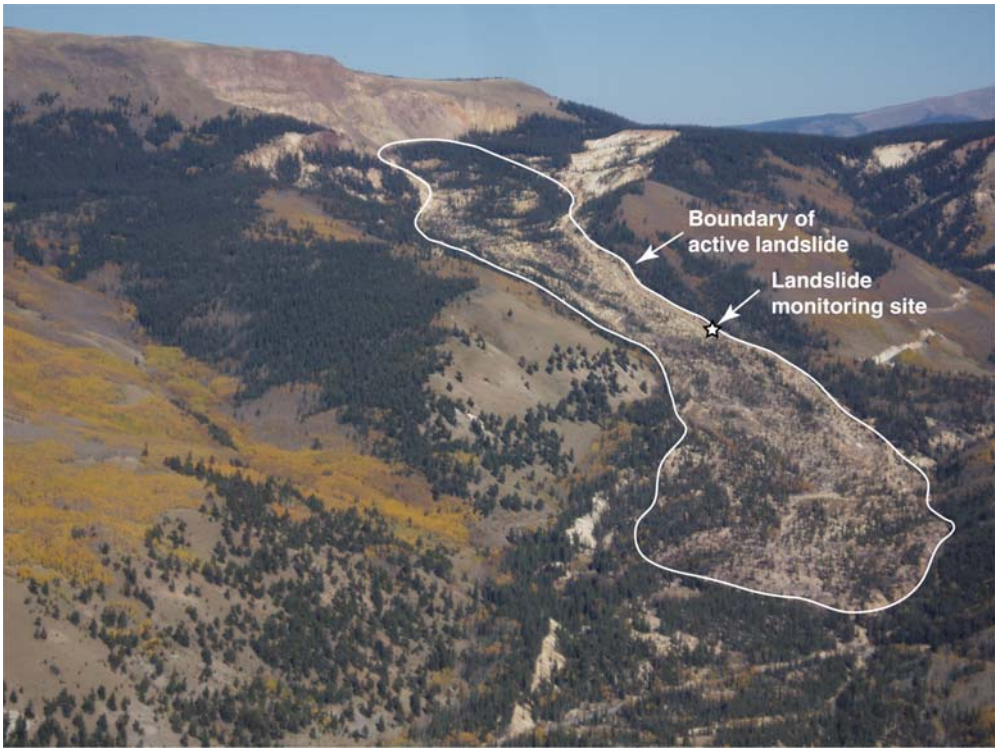

Fig. 2 Photograph showing the active part of the Slumgullion landslide and the location of monitoring equipment. Average width of the landslide is about 300 m and total length is 3.9 km

pressure measured at a depth of 2.2 m and landslide velocity. Baum and Reid (2000) proposed that low-permeability clay layers form along basal and marginal shear zones and impede groundwater flow out of the landslide, thereby aiding continuous displacement by maintaining relatively steady pore-water pressures within the landslide.

Our sampling, field testing, and monitoring were performed at about midlength of the landslide and near its left (when viewed downhill) margin (Figs. 1, 2, and 3) at a monitoring site (IS-1) described by Coe et al. (2003). The monitoring site was located about 100 m downslope from the narrowest, fastest part of the landslide (Fleming et al. 1999; Coe et al. 2003). Average ground surface inclination was 4° within 100 m upslope and downslope from the monitoring site and 10° beyond this distance for a few hundred meters in both directions. Average velocities of about 1.2 cm/day were calculated for areas near the site by evaluating ground-based, time-lapse photographs taken during the summer of 1960 (Crandell and Varnes 1961) and by comparing results from total station surveys performed during 1960 and 1990 (Fleming et al. 1999). An average velocity of about 1.1 cm/day was calculated for the location of the monitoring site by evaluating aerial photographs taken during 1985 and 1990 (Fleming et al. 1999). Most

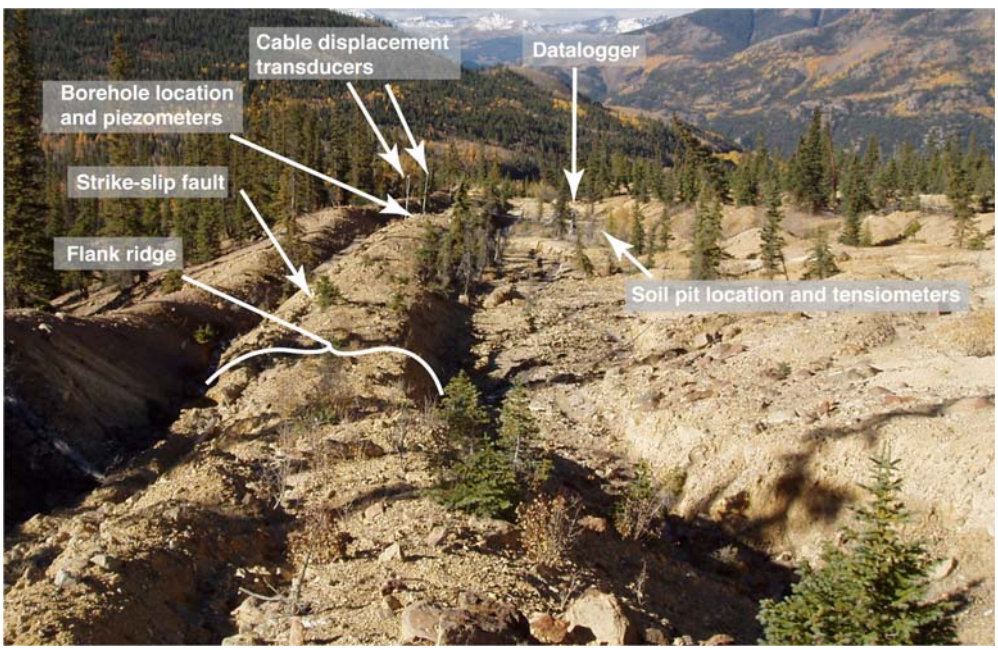

Fig. 3 Photograph of the left (view is oriented downhill) margin of the landslide and the monitoring site. Distance between cable displacement transducers and datalogger is about 15 m

displacement near the monitoring site occurs along a bounding strike-slip fault (Fleming et al. 1999), which was located during the monitoring period about 1 m from the outside of a prominent, 9-m-wide, 2.5-m-high flank ridge (Figs. 3 and 4). This fault is vertical within a meter of the ground surface (maximum depth we excavated). In addition to occurring along a discrete fault, displacement was also observed occurring along en echelon fracture systems within a few hundred meters of the monitoring site.

Methods

Subsurface exploration and sampling

The landslide could only be accessed on foot across steep terrain, so hand-operated equipment was required for drilling boreholes. We used a generator-powered, electric breaker hammer to drive a direct-push boring system made by Geoprobe. We bored a hole 3.4 m from the strike-slip fault that marks the left margin of the landslide and about 4 m from the inside edge of the flank ridge (Figs. 3 and 4). This location was selected to allow observation of groundwater conditions near where shear displacement occurred. The borehole was continuously sampled using a 0.6-m-long, 5.1-cm-diameter, cylindrical steel sampler to a depth of 9.3 m, below which the sampler could not be advanced. The borehole required 9 days to complete. The estimated average depth of the landslide is 13 m (Parise and Guzzi 1992). We also hand-excavated a soil pit to a depth of 1.4 m within the landslide 21 m from its left margin (Figs. 3 and 4). Relatively undisturbed soil samples were obtained from depths of 30, 60, 90, and 120 cm by hand driving 6.3-cm-diameter, 15.2-cm-long, cylindrical brass samplers into the pit walls. Sample disturbance was not quantified. Bulk soil samples were also obtained from these depths.

Material property testing

Grain size distribution, Atterberg limits, specific gravity, water content, and unit weight tests (ASTM International, Standard D 422, D 4318, D 854, D 2216, and D 2937, respectively, 2008) were performed on soil samples obtained from the borehole and soil pit. Soil porosities were calculated from the test results. Saturated hydraulic conductivity of landslide material was measured in situ by performing constant-head borehole permeameter tests (ASTM International, Standard D 5126-90, 2008) at eight locations around the soil pit at depths of 23–89 cm and at two locations along the flank ridge near the borehole at depths of 30 cm.

Monitoring

We installed three, 345-kPa, nonvented, vibrating-wire piezometers manufactured by Slope Indicator, Inc. (±0.345 kPa accuracy) into the borehole to measure pore-water pressures at depths of 4.88, 7.31, and 9.14 m (Fig. 4). These depths were selected to measure pressures near the water table, at a particularly wet zone, and at the bottom of the borehole, respectively (proper inverted installation does not permit the sensor intake to be at the absolute base of the borehole, so the deepest piezometer was installed at a depth of 9.14 m, rather than 9.3 m). The borehole was completely backfilled (hence the nonvented piezometers) with each piezometer being surrounded by sand and isolated from groundwater conditions at neighboring piezometers by at least 0.9 m of bentonite. The upper meter of the borehole was backfilled with cement grout. We installed four Soil Moisture Corp. 100-kPa tensiometers (±0.25 kPa accuracy) into undisturbed soil that formed one of the walls of the soil pit to measure pore-water pressures at depths of 30, 60, 95, and 120 cm (Fig. 4). The pit was then backfilled.

Sensors to measure air temperature, precipitation (rain and snow combined), and snow depth were located 5 m downslope from our soil pit. Air temperature was measured using a Campbell Scientific T107 temperature probe equipped with a radiation shield. Precipitation was measured using a Texas Electronics TE525WS tipping-bucket rain gauge equipped with a Campbell Scientific CS705 snowfall adapter, which melts snow. Snow depth was measured using a Campbell Scientific SR50 ultrasonic distance sensor (±1 cm accuracy).

We used one cable displacement transducer (±0.46 cm accuracy) to measure landslide displacement from July 2, 2004 to June 6, 2006. This transducer was destroyed by wildlife on June 6, 2006 and was replaced by two similar transducers on January 10, 2007. The original transducer and its replacement were located 4 m downslope from our borehole, while the second transducer added during 2007 was located 3 m upslope from our borehole (Fig. 3). We also installed coaxial cable in our borehole to detect the depth of shear displacement, assuming that shear displacement would result in cable breakage at that depth. The length of the coaxial cable (and, therefore, the depth of potential shear-induced cable breakage) was measured periodically using time-domain reflectometry (Kane and Beck 1996) with an accuracy of 30 cm.

All sensors with the exception of the coaxial cable were connected to a solar- and battery-powered Campbell Scientific

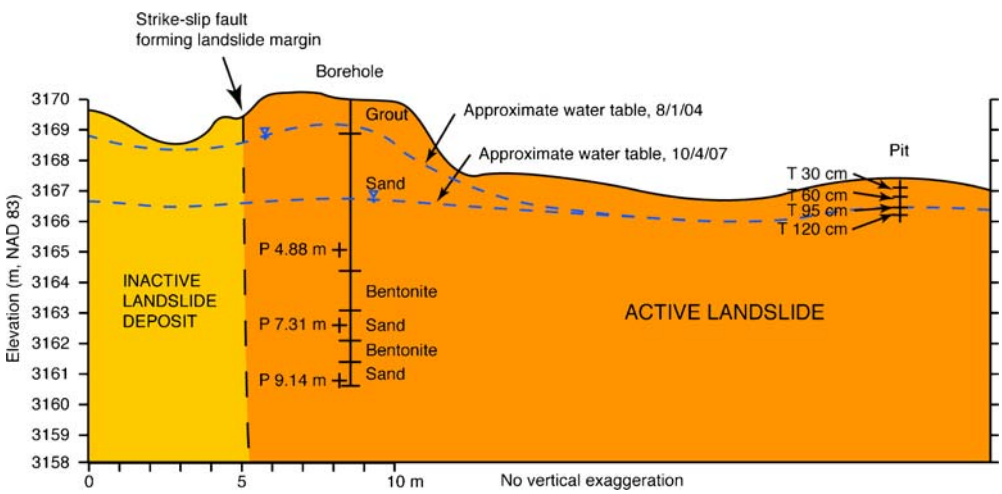

Fig. 4 Cross-section through the monitoring site oriented normal to the landslide margin and directed downhill. "T" indicates tensiometer installed at the depth given and "P" indicates piezometer installed at the depth given. Grout, sand, and bentonite were used to backfill the borehole at the depths indicated

CR10x datalogger. Instrument readings were made hourly and downloaded to a portable computer on a periodic basis. Piezometer readings were corrected for elevation (calibrated at sea level) and temperature, while displacement data were corrected to determine actual landslide displacement (the cable displacement transducers were oriented at acute angles to the direction of landslide displacement; these angles changed continuously during landslide movement). Displacement data were averaged to provide one displacement dataset after the two cable displacement transducers were installed on January 10, 2007.

Results

Soil properties

Soils encountered in the soil pit were classified according to the ASTM Standard D2487 (2008) as homogeneous clayey gravel with sand and were well graded below gravel size (Fig. 5). The average porosity of the four undisturbed soil samples obtained from the soil pit (Table 1) was 0.47. The average in situ hydraulic conductivity measured near the soil pit was 2.32×10^{-5} m/s, which is typical for silty sand to well-sorted sand (Fetter 1994, p. 98).

Soils encountered in the borehole were classified (ASTM International, Standard D2487, 2008) as silty clay, generally with little sand and occasionally with trace gravel. Grain size distributions for samples obtained from the borehole are shown on Fig. 5 and Atterberg limits are provided in Table 1. Samples obtained from depths of 0–1.2 and 8.7–9.3 m were classified as elastic silt and fat clay, respectively. Previous work suggests that the clay consists of smectite and some kaolinite with high swelling potential (Chleborad et al. 1996). All soil obtained from the borehole was generally soft to firm, often laminated, and occasionally fissured. No definite shear surfaces or zones were identified, although some of the laminae were wavy and steeply inclined. These may have been thin shear zones but were not slickensided. The average in situ hydraulic conductivity measured near the borehole was 4.2×10^{-10} m/s, which is near the low end of the range for clay soils (Fetter 1994, p. 98).

Monitoring

Climate

Figure 6 shows measured snow depth and precipitation results. Cumulative precipitation is shown by water year, which begins on October 1, ends on September 30, and is named for the calendar year during which the water year ends. Note that we calculated cumulative precipitation for water year 2004 beginning July 2, 2004 (Fig. 6), so our totals for that year are incomplete.

Water years 2006 and 2007 (Fig. 6) had similar total precipitation that was 135–142% of the water year 2005 total. Precipitation occurred throughout each year, generally as snow during mid-December through mid-April and as rainfall at other times (Fig. 6). The rate of precipitation was relatively low during June and high during March–April and July–early October.

Snowmelt occurred each year during late March through early May (Fig. 6). The abrupt drop in snow depth near the end of February 2006 (Fig. 6) was mostly due to manual removal of snow during equipment maintenance.

Groundwater along the landslide margin

Pore-water pressures measured by the piezometers installed in the borehole located along the landslide margin provided very similar total head values and indicated a fluctuating groundwater table within about 1–3 m of the ground surface (Fig. 6). The vertical hydraulic gradients between the three piezometers ranged from −0.06 to 0.04, thus there appears to have been either static groundwater at the borehole location or primarily horizontal groundwater flow. Because of the similarity between the piezometer measurements and for clarity, the records for only the deepest piezometer (depth of 9.14 m) are shown on the figures (e.g., Fig. 6). Figures 7 and 8 show more detailed data than Fig. 6 and provide a 3-day average piezometer pore-water pressure with the 3-day interval centered on the reported time. This data smoothing was performed to allow direct temporal comparison to smoothed velocity data; velocity data were particularly noisy, as discussed below.

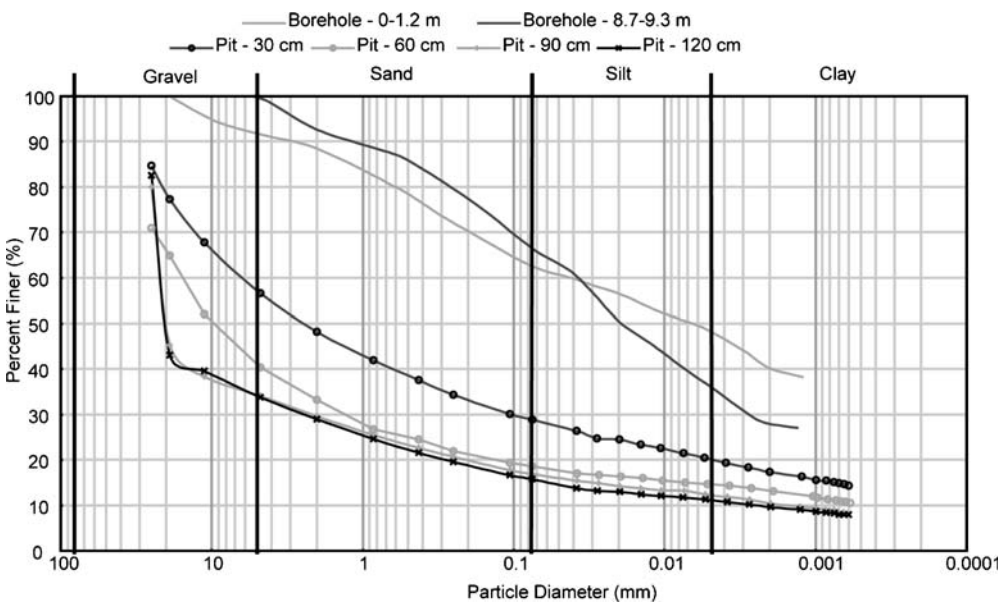

Fig. 5 Grain size distributions of samples obtained from along the landslide margin (borehole samples) and away from the margin (pit samples). Sample depths are indicated in the legend

Table 1 Results of material property testing

Location	Plastic limit	Plasticity index	Hydraulic conductivity (m/s)	Specific gravity	Porosity
Soil pit, 0.30 m depth				2.43	0.40
Soil pit, 0.60 m depth				2.62	0.54
Soil pit, 0.90 m depth				2.50	0.47
Soil pit, 1.20 m depth				2.50	0.48
Borehole, 0–1.2 m depth	41	31			
Borehole, 8.7–9.3 m depth	26	48			
Near soil pit, 0.50 m depth			1.34×10^{-6}		
Near soil pit, 0.23 m depth			4.09×10^{-6}		
Near soil pit, 0.31 m depth			4.26×10^{-6}		
Near soil pit, 0.60 m depth			4.26×10^{-5}		
Near soil pit, 0.89 m depth			4.06×10^{-5}		
Near soil pit, 0.38 m depth			2.00×10^{-5}		
Near soil pit, 0.38 m depth			1.53×10^{-5}		
Near soil pit, 0.35 m depth			5.71×10^{-5}		
Near borehole, 0.30 m depth			2.0×10^{-10}		
Near borehole, 0.30 m depth			6.5×10^{-10}		

Overall, pore-water pressure head along the landslide margin decreased by 2.4 m during the monitoring period but temporarily increased following snowmelt and some rainfall events (Figures 6, 7, and 8). Snowmelt occurred mainly during March and April and the pore-water pressure increase was slow and gradual, continuing into July of each year. Similar to the snowmelt events, several rainfall events were of great enough intensity and duration to produce sustained increases in pore-water pressure along the landslide margin, for example, during late October 2004, late September–mid-October 2005, late July–early August 2006, early October 2006, and mid-July–mid-August 2007 (Fig. 6). Worth noting is that snowmelt- and rainfall-induced pressure increases were preceded by pressure decreases from the beginning of monitoring through the snowmelt period of 2006, but not thereafter (Figs. 6, 7, and 8). This decrease–increase sequence is best illustrated by records from April–May 2005 and 2006 and late September–October 2005. Thus, the pore-pressure responses along the margin to rain or snowmelt changed in character during late 2006 from decrease–increase to increase only.

Groundwater within the landslide away from the margin

Tensiometers located away from the landslide margin (Fig. 4) indicated that the groundwater table was within about a meter of the ground surface in this location throughout the monitoring

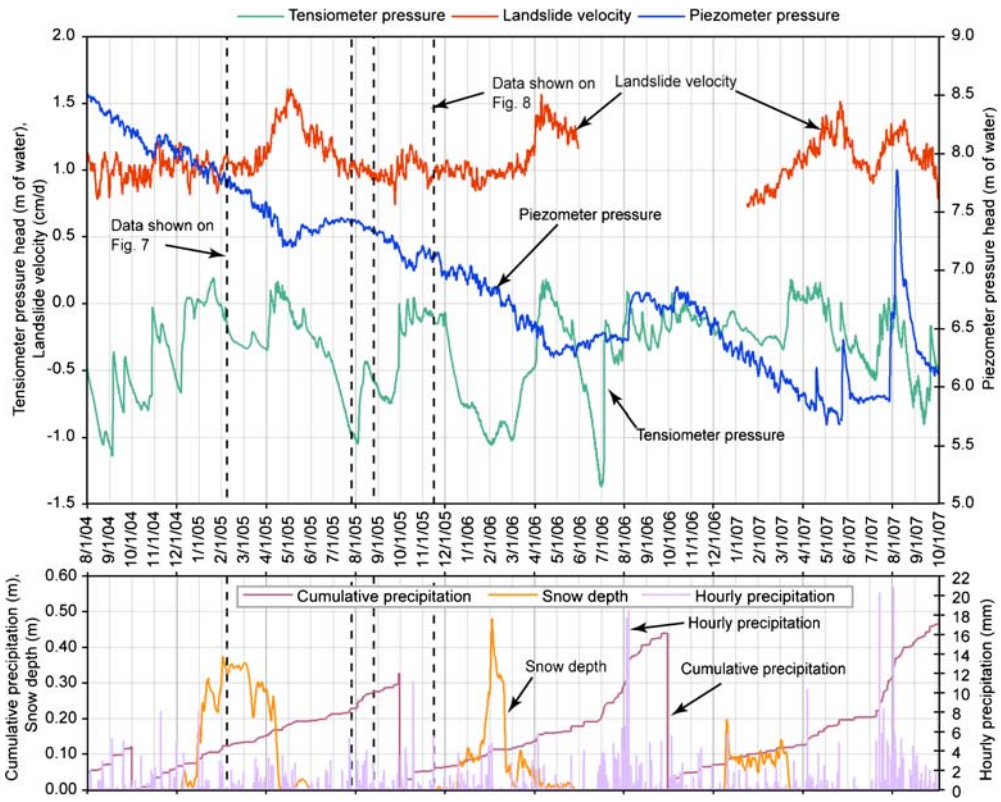

Fig. 6 Chart showing results of monitoring at the landslide, August 1, 2004–October 4, 2007. For clarity, pore-water pressures are shown only for one tensiometer located away from the landslide margin and one piezometer located along the landslide margin. Tensiometer depth is 0.60 m and piezometer depth is 9.14 m

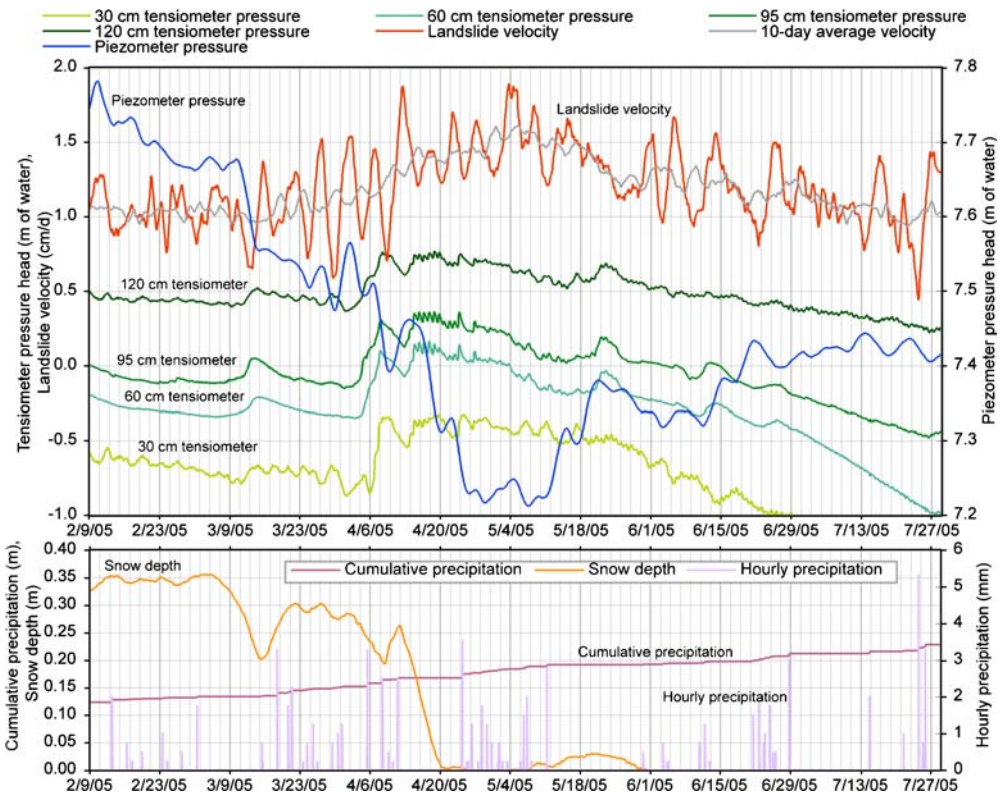

Fig. 7 Chart showing results of monitoring at the landslide, February 9–July 28, 2005. Piezometer depth is 9.14 m. Tensiometer depths are indicated. Snowmelt is suggested when snow depth rapidly decreases (e.g., 4/12/05–4/20/05)

period (record for only one tensiometer at 60 cm depth is shown for clarity; Fig. 6). Changes in pore-water pressures measured by the tensiometers show good temporal correlation with rainfall and snowmelt events. Pore-water pressures were greatest following these events (Fig. 6), but the sequence of tensiometer response was different depending on whether snowmelt (Fig. 7) or rainfall (Fig. 8) occurred. For example, rainfall events were followed by pore-water pressure increases measured first at the shallowest tensiometer and then at progressively deeper tensiometers (e.g., September 30, 2005; Fig. 8), generally within hours to only a few days. In contrast, snowmelt events temporally correlated with simultaneous pore-water pressure increase at all sensors or pore-

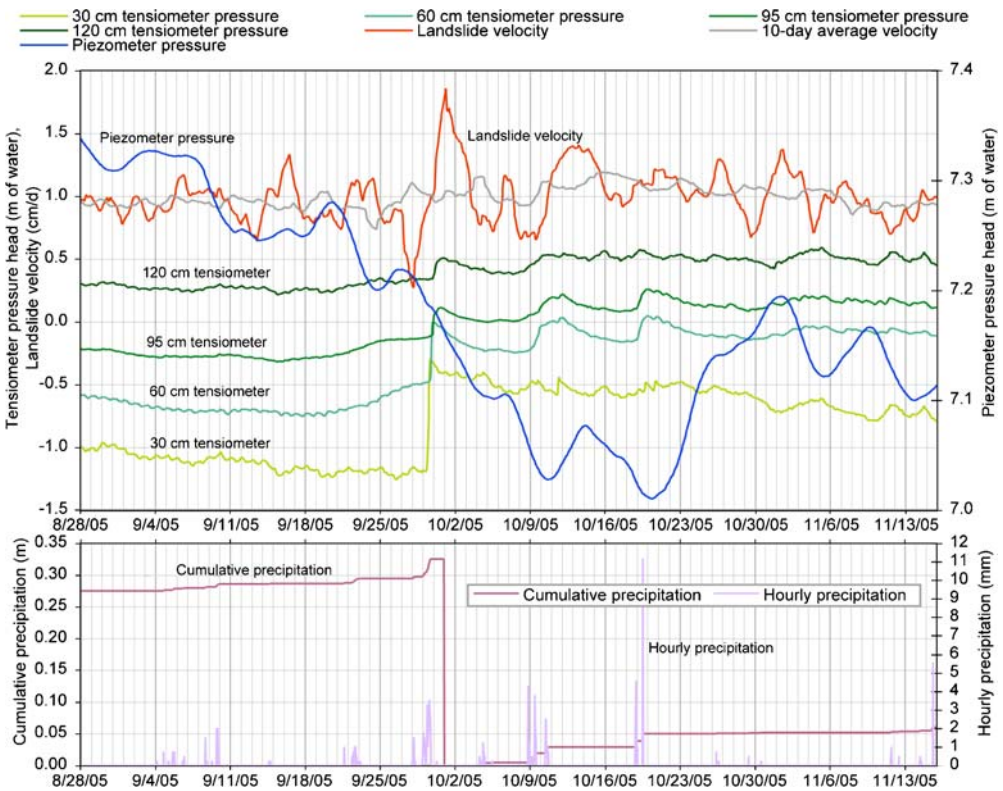

Fig. 8 Chart showing the results of monitoring at the landslide, August 28–November 16, 2005. Piezometer depth is 9.14 m. Tensiometer depths are indicated

water pressure increase observed earliest at greatest depth then at progressively shallower depths (e.g., April 1–6, 2005; Fig. 7).

Landslide displacement and velocity

Episodic monitoring of the coaxial cable installed in our borehole detected no evidence of shear displacement, which indicated that the landslide is deeper than 9.3 m at the location of the borehole. Continuous displacement monitoring indicated that the landslide moved continuously.

Landslide velocity at the monitoring site ranged between 0.7 and 1.9 cm/day with an average of 1.1 cm/day (Figs. 6, 7, and 8). The displacement transducers used to measure velocity included extension cables up to about 53 m long. This length was needed to increase the resolution of landslide displacement by reducing the angle between the cables and the direction of landslide movement; however, the greater length also introduced greater noise in the measurements from environmental effects, such as temperature fluctuations and loading of the cables with wind, rain, snow, and ice. To improve clarity, velocity data shown on the figures were smoothed by calculating average velocities. Figure 6, which shows data from the entire monitoring period, shows the 10-day average of the velocity for each reported time (hourly) with the 10-day interval centered on the reported time. Similarly, Figs. 7 and 8 show the 3- and 10-day average velocities. Time intervals for smoothing were selected arbitrarily with the goal of producing legible charts. Landslide velocity was relatively constant during the monitoring period with the exception of velocities of up to 170% of the overall average that occurred with spring snowmelt and some rainfall events.

Landslide velocity and pore-water pressure

Velocity changes that correlated with snowmelt and rainfall events also generally positively correlated with pore-water pressure changes detected by the tensiometers located within the landslide away from its margin (Fig. 6); periods of elevated pore-water pressure away from the margin correlated with periods of elevated velocity. However, relations between landslide velocity and pore-water pressures detected by the piezometers located along the landslide margin were complex. Pore-water pressure along the margin and significant cycles of landslide acceleration and deceleration showed consistent negative correlation prior to 2007 (Figs. 6, 7, and 8), for example, during March–June 2005, late September–late October 2005, and March–May 2006. During these periods, the landslide accelerated while pore-water pressure dropped and decelerated while pore-water pressure rose. However, this negative correlation was no longer apparent beginning with renewed displacement monitoring during 2007.

Discussion

Although in close proximity, soil properties and relative changes in pore-water pressures differed significantly whether measured along the landslide margin or more than a few meters away from the margin. Soil along the margin is finer-grained (Fig. 5) and has lower hydraulic conductivity (Table 1) than away from the margin, probably due to grain crushing during shear displacement (Agung et al. 2004). The tabular, slickensided clay dikes along which marginal shear displacement was observed likely formed in place also due to grain crushing. Although monitoring of the coaxial cable installed in the borehole alongside the piezometers indicated that the landslide is deeper than our deepest piezometer, the piezometers were installed within the marginal shear zone while the tensiometers were not. Consequently, pore-water pressures (Figs. 6, 7, and 8) measured by the piezometers along the landslide margin were representative for part of the landslide boundary shear zone while the pore-water pressures measured by the tensiometers located away from the landslide margin were representative for part of the landslide body. Although the observations were made within a small area of a very large landslide, differences in observed relations between pore-water pressure and landslide velocity are consistent with and appear to highlight important controls on landslide movement, as discussed below.

Pore-water pressures measured within the landslide body (tensiometer location) abruptly increased following significant rainfall and snowmelt events and decreased in the absence of these events (Figs. 6, 7, and 8), indicating rise and fall of the water table, respectively. The landslide accelerated as the water table rose and decelerated as it fell. These conditions can be explained by using the Coulomb failure rule (e.g., Lambe and Whitman 1969) and Newton's second law of motion:

$$m\,a = \tau - c(\sigma - u)\,\tan\,\phi \qquad (1)$$

where τ is the shear stress along the landslide basal failure surface, c and ϕ are the soil cohesion and angle of internal friction, respectively, σ and u are the total normal stress and pore-water pressure along the failure surface, respectively, m is the landslide mass per unit area of the failure surface, and a is the downslope landslide acceleration. From Eq. 1, an increase of u will result in acceleration and a decrease of u will result in deceleration. For slope-parallel groundwater flow as appears to be generally present, the height of the water table largely controls the value of u, with water table rise resulting in increased u.

In contrast to conditions observed within the landslide body (tensiometer location), pore-water pressures fell within the marginal shear zone (piezometer location) as the landslide accelerated and rose as the landslides decelerated (Figs. 6, 7, and 8). These falling pore-water pressures may have resulted from accelerated shear-induced dilation of soil along the landslide margin during landslide acceleration. Pore-water pressures likely recovered (rose) during deceleration. Shear-induced dilation along landslide margins is common and manifested by en echelon faults and flank ridges (e.g., Fleming and Johnson 1989) as are present at Slumgullion. Dilatant strengthening, reproduced during laboratory testing (Moore and Iverson 2002), field-scale experiments (Iverson et al. 2000), and physically based theoretical modeling (Rudnicki 1984; Iverson 2005), but not previously reported from field observations of a natural landslide, involves shear-induced dilation of dense soil that causes pore-water pressure to fall and effective strengthening of sheared soil if the rate of pore-pressure diffusion is lower than the rate of dilation. According to Iverson et al. (1997), the relative extent to which shear-induced dilation may cause pore-water pressure change may be estimated by:

$$t_{def}/t_{diff} \cong (K\,E)/(\gamma_w\,T\nu) \qquad (2)$$

where t_{def} is the time scale for deformation (in this case, dilation) of the shear zone, t_{diff} is the time scale for pore-pressure diffusion, K and E are the hydraulic conductivity and Young's modulus of the

shear zone, respectively, γ_w is the unit weight of water, T is the thickness of the landslide, and v is the downslope velocity of the landslide. If $t_{def}/t_{diff}<1$, then nonequilibrium pore-water pressures should be produced by deformation of the shear zone during displacement. Using the average measured K of the flank ridge (4.2×10^{-10} m/s), an assumed E of 5 MPa, which is typical for clay (U.S. Army Corps of Engineers 1990), $\gamma_w=9.78\times10^3$ (Lide 1991, assuming groundwater temperature of 10°C), $T=13$ m (Parise and Guzzi 1992), and the average measured v of 1.3×10^{-7} m/s (1.1 cm/day) provides $t_{def}/t_{diff}\cong0.1$. Therefore, the time for pore-pressure diffusion is about ten times greater than that for shear zone deformation, so it appears that movement of the landslide at observed velocities can result in nonequilibrium water pressures within and near shear zones. The pore-water pressure drop induced by landslide acceleration serves to increase resistance to shear displacement and result in landslide deceleration, as shown by Eq. 1. Dilatant strengthening appears to force the landslide to maintain velocities within a relatively narrow range because higher velocities would result in greater pore-pressure imbalance (Eq. 2) and resistance to shear displacement, while lower velocities would result in less imbalance and resistance. Dilatant strengthening may have similarly caused the observed long-term continuous movement at Slumgullion by moderating the effects of longer-term pore-pressure changes, such as would be produced by drought or excessively wet periods. However, excessively wet periods could result in pore-pressure increase that overwhelms the excess negative pore-pressures that result from dilation, thereby resulting in runaway landslide acceleration. This has not yet occurred at the Slumgullion landslide.

There is a significant problem with invoking dilatant strengthening as a mechanism to explain our observations. The theory of dilatant strengthening is predicated on critical-state soil mechanics; shear-induced dilation only occurs until a steady, critical-state soil density is reached (Casagrande 1936). Iverson et al. (1997) reinforce this by indicating that Eq. 2 is valid only prior to reaching critical-state density. If the landslide stopped moving and allowed dilated soil within the shear zone to consolidate, then repeated cycles of dilatant strengthening could occur (Iverson et al. 2000; Moore and Iverson 2002; Iverson 2005), but the landslide has not stopped moving, so critical soil density should have been reached perhaps hundreds of years ago. However, our monitoring results suggest that critical density was only reached near the monitoring site during mid–late 2006; acceleration after this period no longer produced the pore-water pressure drops seen with previous acceleration events. It appears that shear displacement is episodic at fixed locations along the landslide boundaries with "fresh" (denser than critical-state) material episodically being sheared. Episodic displacement at fixed locations is indicated by series of dormant and active flank ridges and abandonment of old and generation of new primary shear surfaces within flank ridges as observed at Slumgullion and other landslides (Fleming and Johnson 1989; Baum et al. 1993; Schulz et al. 2007a, b). Abandoned shear surfaces can consolidate and allow renewed dilation when the soil is again sheared. It seems reasonable, then, to invoke dilatant strengthening along shear zones of some landslides as a mechanism to explain continuous landslide motion within a narrow velocity range, even for landslides that have continuously moved distances beyond that required to achieve critical-state soil density.

Conclusions

The Slumgullion landslide has apparently moved hundreds of meters at a nearly steady rate during the past 300 years. Rate consistency has been directly measured on annual to multiple-year bases beginning in 1960 (Crandell and Varnes 1961; Fleming et al. 1999). Continuous (hourly) measurements of displacement during the past two decades (Savage and Fleming 1996; Coe et al. 2003) show that the landslide maintains a relatively constant rate during most of the year. Pore-water pressures within the landslide away from its margin are also relatively constant, overall. Pore-water pressures away from the margin increase following snowmelt and intense rainfall events and cause reduced resistance to shear displacement along the base of the landslide, resulting in landslide acceleration to as much as 170% of the average velocity. Acceleration is accompanied by decreasing pore-water pressures along parts of the landslide boundaries, and these decreasing pressures serve to increase resistance to shear displacement. This increased resistance causes the landslide to decelerate to its relatively constant velocity. The decreased pore-water pressures along the landslide boundary appear to be caused by soil dilation at rates greater than pore-pressure diffusion, as observed in the laboratory (Moore and Iverson 2002) and in field-scale experiments (Iverson 2005), explained theoretically (Rudnicki 1984; Iverson 2005), and herein explained from field observations. Although the landslide moves continuously, it is likely that dilation along the margins is permitted to continue without reaching critical-state density in all areas due to relocation of primary shear surfaces and reconsolidation of previously dilated soil. Our observations suggest that dilatant strengthening at the Slumgullion landslide is a significant mechanism that regulates landslide motion.

Acknowledgements

We wish to thank Jeff Coe, Rex Baum, Jonathan Godt, William Savage, Brian Collins, Jason Kean, Richard Iverson, and two anonymous reviewers, whose efforts and insight improved this study.

References

Agung MW, Sassa K, Fukuoka H, Wang G (2004) Evolution of shear-zone structure in undrained ring-shear tests. Landslides 2:101–112

ASTM International (2008) Annual book of ASTM standards, 4.08. American Society for Testing and Materials, Philadelphia, PA

Baum RL, Johnson AM (1993) Steady movement of landslides in fine-grained soils—a model for sliding over an irregular slip surface. U.S. Geological Survey Bulletin 1842-D

Baum RL, Reid MR (2000) Ground water isolation by low-permeability clays in landslide shear zones. In: Bromhead E et al (ed) Landslides in research, theory and practice. Thomas Telford, London, pp 139–144

Baum RL, Fleming RW, Johnson AM (1993) Kinematics of the Aspen Grove landslide, Ephraim Canyon. U.S. Geological Survey Bulletin 1842-F, Central Utah

Casagrande A (1936) Characteristics of cohesionless soils affecting the stability of slopes and earth fills. J Boston Soc Civ Eng 23(1):13–32

Chleborad AF, Diehl SF, Cannon SH (1996) Geotechnical properties of selected materials from the Slumgullion landslide. In: Varnes DJ, Savage WZ (eds) The Slumgullion earth flow: a large-scale natural laboratory. U.S. Geological Survey Bulletin 2130, pp 67–71

Coe JA, Ellis WL, Godt JW, Savage WZ, Savage JE, Michael JA, Kibler JD, Powers PS, Lidke DJ, Debray S (2003) Seasonal movement of the Slumgullion landslide determined from Global Positioning System surveys and field instrumentation, July 1998–March 2002. Eng Geol 68:67–101

Coe JA, McKenna JP, Godt JW, Baum RL (2008) Basal-topographic control of stationary ponds on a continuously moving landslide. Earth Surf Processes Landf 34:264–279. doi:10.1002/esp.1721

Corominas J, Moya J, Ledesma A, Lloret A, Gili JA (2005) Prediction of ground displacements and velocities from groundwater level changes at the Vallcebre landslide (Eastern Pyrenees, Spain). Landslides 2:83–96

Crandell DR, Varnes DJ (1961) Movement of the Slumgullion earthflow near Lake City, Colorado. In: Short papers in the geologic and hydrologic sciences. U.S. Geological Survey Professional Paper 424-B, pp B136–B139
Cruden DM, Varnes DJ (1996) Landslide types and processes. In: Turner AK, Schuster RL (eds) Landslides, investigation and mitigation. Special Report 247, Transportation Research Board, National Research Council, Washington, pp 36–75
Diehl SF, Schuster RL (1996) Preliminary geologic map and alteration mineralogy of the main scarp of the Slumgullion landslide. In: Varnes DJ, Savage WZ (eds) The Slumgullion earth flow: a large-scale natural laboratory. U.S. Geological Survey Bulletin 2130, pp 13–19
Fetter CW (1994) Applied hydrogeology. Macmillan, New York
Fleming RW, Johnson AM (1989) Structures associated with strike-slip faults that bound landslide elements. Eng Geol 27:39–114
Fleming RW, Ellen SD, Algus MA (1989) Transformation of dilative and contractive landslide material into material flows—an example from Marin County, California. Eng Geol 27:201–223
Fleming RW, Johnson AM, Messerich JA (1997) Growth of a tectonic ridge. U.S. Geological Survey Open-File Report 97-0153
Fleming RW, Baum RL, Giardino M (1999) Map and description of the active part of the Slumgullion landslide, Hinsdale County, Colorado. U.S. Geological Survey Geologic Investigations Series Map I-2672
Gabet EJ, Mudd SM (2006) The mobilization of debris flows from shallow landslides. Geomorphology 74:207–218
Grainger P, Kalaugher PG (1987) Intermittent surging movements of a coastal landslide. Earth Surf Processes Landf 12:597–603
Hutchinson JN, Prior DB, Stephens N (1974) Potentially dangerous surges in an Antrim mudslide. Q J Eng Geol 7:363–376
Iverson RM (2005) Regulation of landslide motion by dilatancy and pore pressure feedback. Journal of Geophysical Research, 110(F02015)
Iverson RM, Major JJ (1987) Rainfall, ground-water flow, and seasonal movement at Minor Creek landslide, northwestern California: physical interpretation of empirical relations. Geol Soc Amer Bull 99:579–594
Iverson RM, Reid ME, LaHusen RG (1997) Debris-flow mobilization from landslides. Annu Rev Earth Planet Sci 25:85–138
Iverson RM, Reid ME, Iverson NR, Lahusen RG, Logan M, Mann JE, Brien DL (2000) Acute sensitivity of landslide rates to initial soil porosity. Science 290:513–516
Johnson AM (1995) Orientations of faults determined by premonitory shear zones. Tectonophysics 247:161–238
Johnson AM, Rodine JD (1984) Debris flow. In: Brunsden D, Prior DB (eds) Slope instability. Wiley, London, pp 257–361
Johnson AM, Fleming RW (1989) Formation of left-lateral fractures within the Summit Ridge shear zone, 1989 Loma Prieta, California, earthquake. J Geophys Res 98 (B12):21823–21837
Kane WF, Beck TJ (1996) Rapid slope monitoring. Civil Eng 66(6):56–58
Keefer DK, Johnson AM (1983) Earth flows-morphology, mobilisation and movement. U. S. Geological Survey Professional Paper 1264
Lambe TW, Whitman RV (1969) Soil mechanics. Wiley, New York
Lemos LJL (2004) Shear behaviour of pre-existing shear zones under fast loading-insights on the landslide motion. In: Picarelli L (ed) Occurrence and mechanisms of flow-like landslides in natural slopes and earthfills. Pàtrone Editore, Bologna, pp 229–236
Lide DR (ed) (1991) CRC handbook of chemistry and physics. CRC, Boca Raton, FL
Lipman PW (1976) Geologic map of the Lake City caldera area, western San Juan Mountains, southwestern Colorado. U.S. Geological Survey Miscellaneous Investigation Series Map I-962
Locat J, Demers D (1988) Viscosity, yield stress, remolded strength, and liquidity index relationships for sensitive clays. Can Geotech J 25(4):799–806
Madole RF (1996) Preliminary chronology of the Slumgullion landslide, Hinsdale County, Colorado. In: Varnes DJ, Savage WZ (eds) The Slumgullion earth flow: a large-scale natural laboratory. U.S. Geological Survey Bulletin 2130, pp 5–7
Messerich JA, Coe JA (2003) Topographic map of the active part of the Slumgullion landslide on July 31, 2000, Hinsdale County, Colorado. U.S. Geological Survey Open-File Report 03-144
Moore PL, Iverson NR (2002) Slow episodic shear of granular materials regulated by dilatant strengthening. Geology 30(9):843–846
Parise M, Guzzi R (1992) Volume and shape of the active and inactive parts of the Slumgullion landslide, Hinsdale County, Colorado. U.S. Geological Survey Open-File Report 92-216
Prior DB, Stephens N (1972) Some movement patterns of temperate mudflows: examples from Northeastern Ireland. Geol Soc Amer Bull 83:2533–2544
Reynolds O (1885) On the dilatancy of media composed of rigid particles in contact, with experimental illustrations. Philos Mag 5(20):469–481
Rudnicki JW (1984) Effects of dilatant hardening on the development of concentrated shear deformation in fissured rock masses. J Geophys Res 89(B11):9259–9270
Sassa K (1984) The mechanism starting liquefied landslides and debris flows. In: Proceedings of the 4th International Symposium on Landslides, Toronto, University of Toronto Press, Downsview, Canada, pp 349–354
Savage WZ, Fleming RW (1996) Slumgullion landslide fault creep studies. In: Varnes DJ, Savage WZ (eds) The Slumgullion earth flow: a large-scale natural laboratory. U.S. Geological Survey Bulletin 2130, pp 73–76
Schaeffer DG, Iverson RM (2009) Steady and intermittent slipping in a model of landslide motion regulated by pore-pressure feedback. SIAM J Appl Math (in press)
Schulz WH, Highland LM, Ellis WL, Gori PL, Baum RL, Coe JA, Savage WZ (2007a) The Slumgullion landslide, Hinsdale County, Colorado. In: Noe DC, Coe JA (eds) Proceedings of the 1st North American Landslide Conference, Vail, Colorado, June 3–8, Field Trip Guidebooks, Association of Environmental and Engineering Geologists Special Publication Number 21 and Colorado Geological Survey Special Publication 56
Schulz WH, McKenna JP, Biavati G, Kibler JD (2007b) Characteristics of Slumgullion landslide inferred from subsurface exploration, in-situ and laboratory testing, and monitoring. In: Schaefer VR, Schuster RL, Turner AK (eds) Proceedings of the 1st North American Landslide Conference, Vail, Colorado, June 3–8, AEG Special Publication No. 23, pp 1084–1097
Sharp WN, Martin RA, Lane ME (1983) Mineral resource potential of the Powderhorn Wilderness Study Area and Cannibal Plateau Roadless Area, Gunnison and Hinsdale Counties, Colorado. U.S. Geological Survey Miscellaneous Field Studies Map MF-1483-A
Tika TE, Vaughan PR, Lemos LJL (1996) Fast shearing of pre-existing shear zones in soil. Geotechnique 46(2):197–233
U.S. Army Corps of Engineers (1990) Engineering and design, settlement analysis: engineer manual 1110-1-1904. U.S. Army Corps of Engineers, Washington
van Asch ThWJ, Van Beek LPH, Bogaard TA (2007) Problems in predicting the mobility of slow-moving landslides. Eng Geol 91:46–55
Varnes DJ, Savage WZ (eds) (1996) The Slumgullion earth flow: a large-scale natural laboratory. U.S. Geological Survey Bulletin 2130
Vulliet L, Hutter K (1988) Viscous-type sliding laws for landslides. Can Geotech J 25 (3):467–477
Wang G, Sassa K (2003) Pore-pressure generation and movement of rainfall-induced landslides: effects of grain size and fine-particle content. Eng Geol 69:109–125

W. H. Schulz (✉) · J. P. McKenna · J. D. Kibler
U.S. Geological Survey,
M.S. 966, P.O. Box 25046, Denver, CO 80225, USA
e-mail: wschulz@usgs.gov

G. Biavati
Università di Bologna,
Via Zamboni 67,
40126 Bologna, Italy